Kinetics and Equilibria in Ligand Binding by Nitrophorins 1−4: Evidence for Stabilization of a Nitric Oxide−Ferriheme Complex through a Ligand-Induced Conformational Trap†

John F. Andersen,‡ Xiao D. Ding,§ Celia Balfour,‡,§ Tatjana Kh. Shokhireva,§ Donald E. Champagne,|| F. Ann Walker,§ and William R. Montfort*,‡

Departments of Biochemistry and Chemistry, University of Arizona, Tucson, Arizona 85721, and Department of Entomology, University of Georgia, Athens, Georgia 30602

Received April 4, 2000

ABSTRACT: Nitrophorins 1−4 (NP1−4) are ferriheme proteins from the blood-sucking insect *Rhodnius prolixus* that transport nitric oxide (NO) to the victim, sequester histamine, and inhibit blood coagulation. Here, we report kinetic and thermodynamic analyses for ligand binding by all four proteins and their reduction potentials. All four undergo biphasic association and dissociation reactions with NO. The initial association is fast (1.5−33 μM^{-1} s^{-1}) and similar to that of elephant metmyoglobin. However, unlike in metmyoglobin, a slower second phase follows (∼50 s^{-1}), and the stabilized final complexes are resistant to autoreduction ($E° = +3$ to $+154$ mV vs normal hydrogen electrode). NO dissociation begins with a slow, pH-dependent step (0.02−1.4 s^{-1}), followed by a faster phase that is again similar to that of metmyoglobin (3−52 s^{-1}). The equilibrium dissociation constants are quite small (1−850 nM). NP1 and NP4 display larger release rate constants and smaller association rate constants than NP2 and NP3, leading to values for K_d that are about 10-fold greater. The results are discussed in light of the recent crystal structures of NP1, NP2, and NP4, which display open, polar distal pockets, and of NP4−NO, which displays an NO-induced conformational change that leads to expulsion of solvent and complete burial of the NO ligand in a now nonpolar distal pocket. Taken together, the results suggest that tighter NO binding in the nitrophorins is due to the trapping of the molecule in a nonpolar distal pocket rather than through formation of particularly strong Fe−NO or hydrogen bonds.

The nitrophorins (NPs)[1] are a group of four heme proteins from the saliva of the blood-feeding insect *Rhodnius prolixus*, which carries the trypanosome responsible for Chagas' disease in South America (*1*). These proteins facilitate feeding by interfering with hemostasis in the mammalian host by three distinct mechanisms (reviewed in refs *2* and *3*). First, the NPs contain a nitric oxide (NO) ligand bound to heme when isolated from the salivary secretion, which is readily lost on dilution in the host skin, where it serves as a vasodilator in the vicinity of the bite (*4*). Second, the NPs also bind tightly to histamine in the same binding pocket as for NO (*5*, *6*). Mast cells in the vicinity of the bite release large quantities of histamine in response to the insect bite. Binding of this ligand by the NPs serves to displace the nitric oxide ligand, resulting in more efficient vasodilatory activity, and also serves to dampen histamine-induced inflammation. Third, one of the four NPs, NP2, possesses an anticoagulant activity through direct inhibition of factor X maturation (*7*, *8*). This activity does not involve the NP2 heme.

The *Rhodnius* NPs are quite similar and display 38% sequence identity. The proteins, however, fall into two groups based on sequence identity: NP1/4 (90% identical) and NP2/3 (79% identical). The X-ray crystal structures of NP1 (*6*), NP2 (*26*), and NP4 (*9*) show that the NPs consist of an eight-stranded β-barrel with a b-type heme placed deep into one end of the barrel. The overall fold is characteristic of the lipocalin protein family that also contains retinol-binding protein, β-lactoglobulin, and bilin-binding protein (reviewed in ref *3*). Although the NP structure is unique for a hemoprotein, a histidine residue acts as the proximal axial ligand to the heme iron in an arrangement similar to that of the globins.

The focus of the present study is on the mechanism by which NO is protected, transported, and released to the host by the NPs. The use of heme for this function is interesting in that NO is quite reactive and binds nearly irreversibly to the heme of myoglobin (reviewed in ref *10*). To function, the NP heme must be stabilized in the Fe(III) (ferric) state, where NO affinity is in the micromolar range and release to the victim is favorable, rather than in the Fe(II) (ferrous) state that is the natural state of the globins, where NO affinity is in the picomolar range and release is disfavored (*11*). That

† This work was supported in part by National Institutes of Health Grants GM58727 (J.F.A.), AI35591 (D.E.C.), and HL54826 (W.R.M. and F.A.W.), ACS Grant RPG-93-041-04-CDD (W.R.M.), and ADCRC Grant 1-208A (W.R.M).

* Corresponding author: e-mail montfort@u.arizona.edu; telephone 520-621-1884; fax 520-621-1697.

‡ Department of Biochemistry, University of Arizona.

§ Department of Chemistry, University of Arizona.

|| Department of Entomology, University of Georgia.

[1] Abbreviations: NP1−4, *Rhodnius* nitrophorins 1−4; NO, nitric oxide; K_d, spectral ligand dissociation constant; k_{off}, overall dissociation rate constant; k_{obs}, individual observed rate constant; K_{-1}, k_{-1}/k_1 for nitric oxide; K_{-1H}, k_{-1H}/k_{1H} for histamine; NP^{II}, ferrous nitrophorin; NP^{III}, ferric nitrophorin; sGC, soluble guanylate cyclase.

10.1021/bi000766b CCC: $19.00
Published on Web 07/26/2000

the NP−NO complexes are indeed stabilized in a low-spin ferric state has been shown by EPR spectroscopy (*4*, *9*, *12*). Furthermore, the NP1−NO complex is not subject to rapid autoreduction (*12*), unlike the case for the Fe(III) center in methemoglobin (*13*, *14*) or metmyoglobin at higher pH (*15*), suggesting the NO ligand is somehow protected from solvent while it is stored complexed with the NPs in the insect salivary gland.

The kinetics and pH dependence for NO release from insect-derived NPs (*4*, *16*) and from recombinant NP1 (*16*) and NP2 (*17*) have been reported. These studies found that NO release is faster at the physiological pH of the host (∼7) than at the pH of the insect saliva (∼5), a feature that is of likely importance for efficient NO transport. The studies also revealed NO release by the NPs to differ from release by metmyoglobin in that the release rates are relatively slow—especially at lower pHs—and biphasic. The mechanism by which NO release rates are reduced and made pH dependent, as well as the way in which the NP−NO complex is protected from autoreduction, has been unclear, since much of the structural and spectroscopic data suggest just the opposite should occur. For example, the NO binding pocket was found to be quite open to solvent in the first several NP structures determined, and the NP1−NO bond was found to be typical for ferric nitrosyl complexes at all pHs, on the basis of stretching frequencies examined by infrared spectroscopy (*12*). Also, the NP1 reduction potential, although more negative than that for metmyoglobin, varies only slightly with pH (*12*).

A partial explanation for this apparent inconsistency is suggested by our recent structure determination of the NP4−NO complex, in which a remarkable feature was revealed: the binding of NO leads to the collapse of two loops into the binding pocket, allowing hydrophobic residues to pack against the NO ligand and releasing several solvent molecules from the pocket (Figure 1; *18*). As a result, NO is completely buried by hydrophobic residues, and what was an open, relatively hydrophilic binding pocket in the absence of NO is now closed and largely hydrophobic. It is not yet clear how these dramatic changes in structure give rise to altered release rates, since (1) the NP NO−heme bond appears typical for ferric nitrosyl complexes by IR spectroscopy, at least for NP1 (*12*); (2) the loops filling the binding pocket are quite dynamic, on the basis of the crystallographic temperature factors (*18*); and (3) diatomic molecules are known to move nearly as rapidly through proteins, due to rapid structural fluctuations, as they do through water (*19*).

In the present study, we have undertaken kinetic and thermodynamic characterizations of NO and histamine binding to recombinant forms of all four NPs. The studies provide the first complete analyses for any of these proteins and link the dynamic properties of the family to their X-ray structures. From these studies, a model emerges where the slow rate of NO release is due to a hydrophobic trapping of the ligand in the distal pocket, induced by loop closure. The rate-determining and pH-dependent step appears to be loop opening for all four proteins. Consistent with this model are the slower off rates and the higher overall affinity constants of NO with NP2/3 as compared with NP1/4, since the NP2/3 binding pocket is more hydrophobic (*26*). These differences among the NPs may be of functional importance in vivo as well, since it allows the insect to deliver NO over a wide range of time with a single injection of NP4−NO-containing saliva.

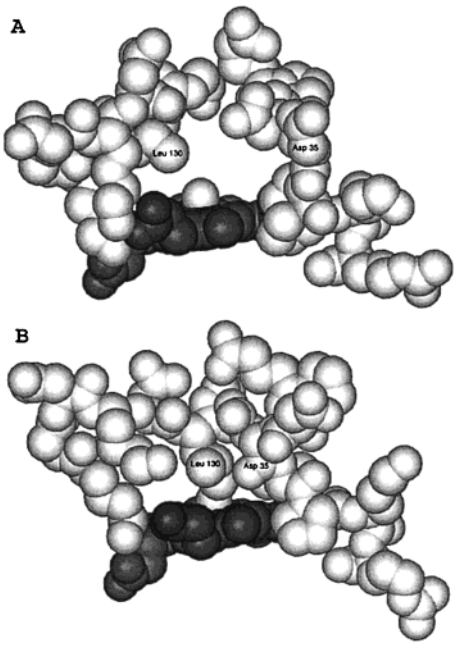

FIGURE 1: Conformational changes in the crystal structure of NP4 on NO binding (*18*). (A) NP4−NH_3; (B) NP4−NO. The A−B and G−H loops and the distal ligand are shown in gray, and the heme in black. Residues Asp 35 (A−B loop) and Leu 130 (G−H loop) are labeled, and ordered water molecules in the distal pocket have been omitted for clarity. The A−B and G−H loops shift upon NO binding to bury the ligand and block access to the distal pocket. Asp 30 (hidden in this view) is also buried in this transition.

MATERIALS AND METHODS

Preparation of Proteins. Recombinant NP1 and 4 were prepared from *Escherichia coli* as described previously (*9*, *16*). The proteins were expressed as inclusion bodies that were solubilized in a buffer containing guanidine hydrochloride and renatured by dilution into a buffer containing high concentrations of DTT. After refolding, hemin was added to the mixture and DTT was removed to allow the disulfide bonds to form. NP2 and NP3 initially showed poor expression in *E. coli*, so modifications were made in the 5′ end of the coding sequence to improve the similarity to *E. coli* codon usage. The PCR primers GGGAATTCCATATGGACTGTAGCACCAACATCAGCCCGAAACAGGGTCTGGATAAAG and GGGAATTCCATATGGACTGTAGCACCAACATCAGCCCGAAAAAAGGTCTGGATAAAG for NP2 and NP3, respectively, were used to modify the 5′ end without modifying the amino acid sequence of the protein. The modified cDNAs were placed into pET17b for expression in the strain BL21 (DE3), and protein was prepared from inclusion bodies, as previously described for NP1 and NP4 (*9*, *16*), except that the NP2 and NP3 proteins were passed through a column of Q-Sepharose after addition of heme, followed by chromatography on Sephacryl S-100. This procedure yields about 2 mg/L of cultured cells. Analysis by Edman degradation and mass spectrometry indicate the presence of methionine at the N-terminus of NP1, NP2, and NP3 and the lack of an N-terminal methionine for NP4. In the insect, the proteins are processed from a precursor containing a signal peptide, so none of the four

contains an N-terminal methionine in the mature form of the insect-produced protein. At this point, it is not known if the presence of methionine has a functional effect.

Kinetic Studies. Stopped-flow measurements of NO or histamine binding with NPs were performed on a High-Tech SF51 stopped-flow apparatus (3 ms dead time) coupled with an Olis optical detection system. Saturated solutions of nitric oxide (concentration 1.9 mM at 1 atm) were prepared by passing NO gas through buffer solutions that had been deoxygenated through bubbling with oxygen-free argon. Dilutions of saturated nitric oxide were made in gastight syringes with argon-purged buffers. Changes in absorbance at 400 nM were observed and the data were fit with either a single exponential (NP1 and NP4), or a sum of two exponentials (NP2 and NP3) by the Marquardt algorithm as encoded in SigmaPlot (Jandel Scientific), to yield the observed rate constants.

Scheme 1

$$\mathrm{NP} + \mathrm{L} \underset{k_{-1}}{\overset{k_1}{\rightleftharpoons}} \mathrm{NP{-}L}$$

The monophasic reactions of NP1 and NP4 with ligands are described by Scheme 1, where L refers to either NO or histamine. The second-order rate constants for ligand binding (k_1) and the reverse rate constants (k_{-1}) were obtained from the concentration dependence of k_{obs} by fitting to eq 1 (*20*):

$$k_{obs} = k_1[\mathrm{L}] + k_{-1} \quad (1)$$

where [L] is the concentration of NO or histamine.

Scheme 2

$$\mathrm{NP} + \mathrm{L} \underset{k_{-1}}{\overset{k_1}{\rightleftharpoons}} \mathrm{NP{-}L} \underset{k_{-2}}{\overset{k_2}{\rightleftharpoons}} \mathrm{NP'{-}L}$$

The biphasic association kinetics of NP2 and NP3 were analyzed as a two-step reaction in which the first step is represented by the fast phase of the reaction (Scheme 2). The rate constants k_1 and k_{-1} were obtained from the fast reaction phase and determined by use of eq 1, where k_{obs} in this case was the observed pseudo-first-order rate constant for the fast phase of the biphasic reaction. The first-order rate constant k_2 was determined by fitting eq 2 with the assumption that k_{-2} is small relative to k_2 and k_{-1} (*20*):

$$k_{obs} = k_1k_2[\mathrm{L}]/(k_1[\mathrm{L}] + k_{-1} + k_2) \quad (2)$$

where k_{obs} is the observed first-order rate constant for the slow phase of the binding reaction. Due to the small measurable amplitude of the second phase and its ligand concentration dependence, the values for k_2 are only estimates and were only obtainable in any case for NP2 and NP3.

Scheme 3

$$\mathrm{NP{-}NO} + \mathrm{Hi} \underset{k_1}{\overset{k_{off}}{\rightleftharpoons}} \mathrm{NP} + \mathrm{NO} + \mathrm{Hi} \underset{k_{-1H}}{\overset{k_{1H}}{\rightleftharpoons}} \mathrm{NP{-}Hi} + \mathrm{NO}$$

The overall dissociation rate constant for release of NO from the NP−NO complex (k_{off}) was estimated by measuring the rate of the displacement reaction with histamine (Hi). Histamine binds to the NPs with high affinity, binds rapidly relative to NO under conditions of large histamine excess, and leads to a shift in the Soret maximum from near 420 nm for the NO complex to near 413 nm for the histamine complex. The first-order rate constant for NO release in the displacement reaction can be estimated from

$$k_{obs} = k_{off}/[1 + (k_1[\mathrm{NO}]/k_{1H}[\mathrm{Hi}])] \quad (3)$$

in which k_{obs} is the observed first-order displacement rate constant for the change in absorbance at 423 nm, k_1 is the bimolecular rate constant for NO binding (from eq 1), k_{1H} is the bimolecular rate constant for histamine binding, and k_{off} is the overall NO dissociation rate constant (*21*). The value for k_{-2} (Scheme 2) was estimated from k_{off} by use of

$$k_{-2} = k_{off}(k_{-1} + k_2)/(k_{-1} - k_{off}) \quad (4)$$

All four NPs were found to display two phases for k_{off}, referred to as k_{off1} and k_{off2}. An overall k_{off} for use in eq 4 was estimated as the sum of the two phases after each phase was weighted by its corresponding amplitude. Under conditions where more rapid release rates occurred, for example with NP1 and NP4 at pH 8.0, measurements were made with a stopped-flow apparatus. In these instances, equal volumes of NP−NO complex (generally 10 μM) and histamine solution (1−10 mM) in identical buffers were added to the syringes of the instrument. For less rapid release rate measurements, 10 μL of concentrated histamine solution was added to 1 mL of NP−NO complex in a sealed cuvette, the solution was rapidly mixed, and the absorbance at 423 nm was monitored in a Shimadzu UV160U spectrophotometer. For these experiments, the NP−NO complex was formed by adding a saturated solution of NO to the sealed cuvette containing 10 μM NP in the desired buffer to give a final NO concentration of 15 μM. No change in displacement rates was found when experiments were repeated with histamine concentrations varied within the 1−10 mM range.

Flash photolysis measurements were carried out with a Photochemical Research Associates nitrogen dye laser with a pulse width of approximately 500 ps, using POPOP (0.39 g/mL) in toluene as the dye. Transients were recorded, digitized, and averaged on a Tektronix TDS 410A oscilloscope.

Equilibrium Binding Measurements. Equilibrium measurements were made by optical difference spectrophotometry to measure the shift in the Soret absorbance position on binding either nitric oxide or histamine. Experiments were performed in 5.0 cm path length cells using protein concentrations as low as 5 nM. Absorption by the sample was too small at lower concentrations for binding to be measured, and thus equilibrium constants could not be obtained for NP2−NO at low pH. Measurements were performed on a Cary 15−Olis spectrophotometer at 25 °C. To calculate the spectral dissociation constant (K_d), the peak-to-trough differences of the absorbance maximum (approximately 423 nm for NO and 413 nm for histamine) and minimum (approximately 404 nm) for ligand-bound minus ligand-free difference spectra, were calculated and plotted vs ligand concentration (*16*). The data were fitted with

$$\Delta A = B[\mathrm{L}]/([\mathrm{L}] + K_d) \quad (5)$$

where ΔA is the differential absorbance and B is the maximal value for the differential absorbance. To determine apparent

pK_a for the transition from low to high affinity, the data were fit to eq 6 for a titration curve (*22*):

$$K_d = [K_{dmin} + (K_{dmax}10^{pH-pK_a})]/(1 + 10^{pH-pK_a}) \quad (6)$$

where K_{dmin} and K_{dmax} are the asymptotic minimum and maximum K_d values, respectively.

Electrochemical Measurements. The reduction of NP2−4 and their NO complexes, and the histamine complexes of all four NPs, were investigated by spectroelectrochemical techniques as described previously for NP1 and its NO complex (*12*) with a BAS CV-50W voltammetric analyzer and a Spectral Instruments spectrophotometer, both under computer control. The optically transparent thin-layer working electrodes (OTTLE), counterelectrodes, and reference electrode were the same as used previously (*12*). Solutions of the protein plus mediators and buffer were prepared and degassed as described previously (*12*), and spectra were recorded over the same potential ranges as previously for NP1 and NP1−NO (*12*). The protein concentration used (∼50−60 μM) was well above the NP^{III}−NO dissociation constants for all pH values studied. The temperature was 27 + 1 °C.

The spectroelectrochemical titrations were carried out by setting the potential at some value $E°'$ and waiting until the optical spectrum did not change with time, then recording the optical spectrum, followed by setting a new potential $E°'$ and repeating the process, etc. The data were analyzed in terms of the Nernst equation, which describes the effect of applied potential on the ratio of the concentrations of oxidized and reduced forms of the complex and the true reduction potential, $E°$:

$$E°' = E° + 2.303(RT/nF) \log ([ox]/[red]) \quad (7)$$

where $E°'$ is the applied potential, $E°$ is the reduction potential determined from these data, and [ox] and [red] are the concentrations of the protein in the Fe(III) and Fe(II) states, respectively, in the presence of either no ligand or a high enough concentration of ligand L to ensure full complexation of both oxidation states. [Ox] and [red] are calculated from the optical spectra by use of Beer's law. $E°$ is determined as the intercept of the plot of log ([ox]/[red]) vs applied potential $E°'$. The slope of this plot is $2.303RT/nF = 59$ mV at 25 °C or 59.5 mV at 27 °C. In all cases, the observed slopes were 60 ± 2 mV.

The shift of the Fe^{III}/Fe^{II} reduction potential when a ligand L is bound to the iron is a measure of the ratio of the Fe−L dissociation constants for the two oxidation states, since the Nernst equation (eq 7) can be rewritten as

$$E°_c = E° + (RT/nF) \ln (K_d^{III}/K_d^{II}) \quad (8)$$

where $E°_c$ is the measured potential for the nitrophorin fully complexed to the ligand L, $E°$ is the measured potential for the nitrophorin in the absence of L, and K_d^{III} and K_d^{II} are the dissociation constants for ligand L from the Fe(III) and Fe(II) states, respectively. From eq 8, the ratio of the dissociation constants for the two oxidation states is thus $\exp[-(E°_c - E°)F/RT]$.

RESULTS

Expression and Spectral Features of NPs. Expression and purification of NP2 and NP3 was similar to that previously described for NP1 and NP4 (*9*, *16*) (see Materials and Methods for details). Like NP1 and NP4, the optical spectra of unliganded NP2 and NP3 show a Soret maximum at 403−404 nm. On binding NO, the Soret band shifts to 419−420 nm in NP1 and NP4 (*9*, *12*, *16*) and 421 nm in NP2 and NP3 (Figure 2). The α and β bands of the NO-complexes are located near 570 and 535 nm, respectively, for all four proteins. The histamine complexes of the NPs have Soret maxima at 410−412 nm and broad maxima between 580 and 520 nm. Shifts in the Soret maximum on addition of ligands were used to measure the equilibrium binding and binding kinetics of NO and histamine with the NPs.

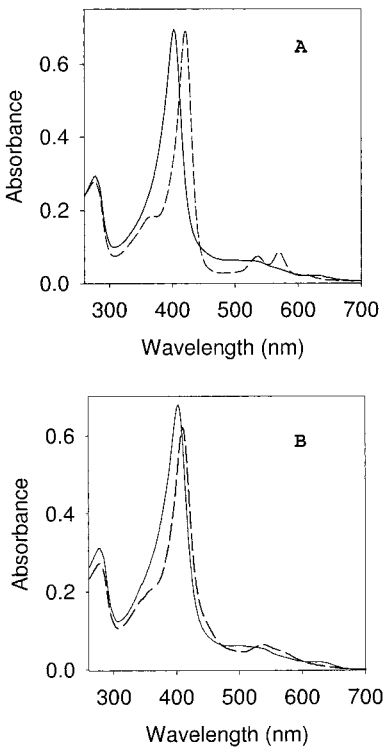

FIGURE 2: Absorption spectra for NP2 and NP3. (A) UV−visible spectra of recombinant NP2 either without ligand (—) or as the NO complex (- - -). (B) UV−visible spectra of NP3 either without ligand (—) or as the histamine complex (- - -).

Scheme 4

$$NP + NO \underset{k_{-1}}{\overset{k_1}{\rightleftharpoons}} NP{-}NO \underset{k_{off1}/k_{off2}\ (pH\text{-}dep)}{\overset{k_2}{\rightleftharpoons}} NP'{-}NO + NP''{-}NO$$

Overview of NP Ligand Binding Kinetics. The nitrophorins are single-domain heme proteins about the same size as myoglobin. Yet, unlike for myoglobin or metmyoglobin, the kinetics of NP ligand binding and release are biphasic and pH-dependent, suggesting a more complex binding mechanism occurs in the nitrophorins. In the present study, we developed a number of approaches for determining kinetic and thermodynamic constants for NO binding and release by the nitrophorins, which led to the detection of three distinct NP−NO species, referred to as NP−NO, NP′−NO, and NP″−NO. The relationships between these forms, based on the results to be presented below, are summarized in Scheme 4 where k_2 refers to a stabilizing event that occurs after initial binding (most likely the NO-induced conformational change), and k_{off1} and k_{off2} refer to fast and slow

observed release rate constants that are related to k_{-1} and k_{-2} in a manner that is not yet fully clear. NP′−NO and NP″−NO designate the two forms of the NP−NO complex that give rise to k_{off1} and k_{off2}. The relationship between NP′−NO and NP″−NO, and whether they represent interconvertible forms of the complex, is not yet known.

To measure ligand binding, the shift in the Soret band was monitored after rapid mixing of protein and ligand in a stopped-flow device or by monitoring rebinding after laser flash photolysis-induced dissociation of the complex. The binding rate constants k_1 and k_2 (for NP2) were obtained from these data, as well as the ligand dissociation rate constant k_{-1}, by use of eqs 1 and 2 (see Materials and Methods). The overall ligand dissociation rate constants (k_{off}) were measured by rapid mixing of NP−NO with excess histamine, either in a standard cuvette or in a stopped-flow device. Replacement of NO by histamine was monitored by the Soret shift between the two complexes, and the true off rate was obtained from the histamine displacement rates by use of eq 3. As noted, two dissociation rate constants were detected for each NP.

Overall dissociation constants (K_d) were measured directly by monitoring the shift in the NP Soret band as a function of increasing ligand concentration and also estimated by the appropriate combination of rate constants where possible.

NO Association Reactions. The binding of NO to all four nitrophorins was examined by stopped-flow methods. The binding kinetics for NP2 and NP3 were similar and clearly biphasic (Figure 3A), while two phases could not be clearly resolved for NP1 and NP4 (Figure 4A). NO binding to NP1/4 and the fast phase for binding to NP2/3 showed linear NO concentration dependencies, consistent with a bimolecular reaction (Figures 3B and 4B). The association rate constants were not highly pH-dependent for any of the nitrophorins, and biphasic kinetics were seen for NP2 and NP3 at all pHs examined. Thus, the pH dependence for NO binding affinity is not a function of the association reaction.

The values for k_1 were approximately 10-fold smaller for NP1/4 than for NP2/3 (Table 1) and similar to that seen for elephant metmyoglobin, which has a relatively unencumbered path for NO binding (*23*). Sperm whale metmyoglobin, which has a stabilized water molecule ligated to the heme iron, displays on rates 40−400-fold slower than those of the nitrophorins (Table 1). Thus, the nitrophorins have an initial NO association rate consistent with an unencumbered binding pocket.

The amplitude of the slow binding phase in NP2 and NP3 diminishes as the NO concentration is increased and shows little NO concentration dependence (Figure 3B). Kaneko et al. (*17*) have also observed this slow phase and attribute it to the conversion of an initial complex formed in the fast phase to a stabilized complex, by a sequential mechanism. We have analyzed the NP2 and NP3 binding data with this model in mind (Scheme 2, Materials and Methods) and have used the maximal value of k_{obs} for the slow phase as an estimate of k_2 (Table 1). The slow absorbance change apparently represents a perturbation of the equilibrium for formation of the initial complex (NP−NO) at NO concentrations that are subsaturating for the initial complex, i.e., near K_{-1} ($= k_{-1}/k_1$). Formation of NP′−NO at NO concentrations near K_{-1} allows more NP−NO to form by continually removing this complex from the system. This manifests itself as a rapid absorbance change (fast phase) representing the formation of NP−NO and limited by K_{-1}, followed by a slow absorbance change (slow phase) representing the conversion of NP−NO to NP′−NO.

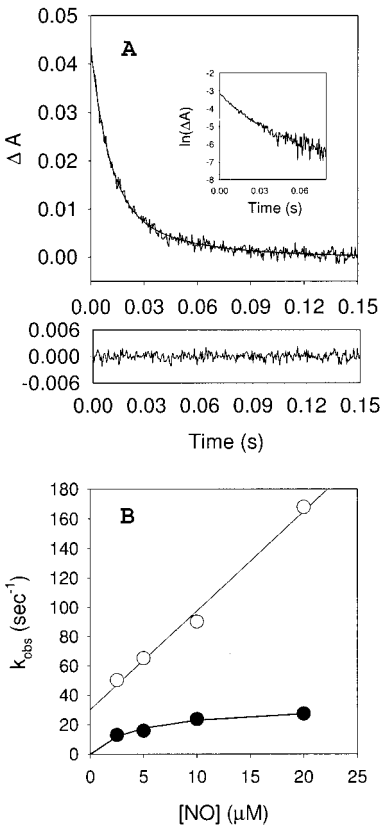

FIGURE 3: NO complex formation with NP2 and NP3 detected by stopped-flow mixing. (A) Association reaction of NO (10 μM) with NP2 at 12 °C, pH 5.0, and monitored at 400 nm. The data were fit to a double exponential decay. Plots of ln (ΔA) vs time (inset) and the regression residuals (below) confirm the biphasic rate behavior. (B) NO concentration dependence of k_{obs} for NP3 at pH 8.0 and 12 °C. The fast phase data (○) were fit to eq 1, yielding k_1 and k_{-1}. The slow phase data (●) were fit to eq 2, yielding k_2.

Although a second phase is not measurable in NP1 and NP4, a slow binding step is indicated by the small values obtained for K_d and k_{off} in experiments described below. If there were no slow binding step, these constants would be equal within experimental error to K_{-1} and k_{-1}; however, the values for K_d are 3−45-fold smaller than for K_{-1}, depending on pH, and the values for k_{off} are 3−88-fold smaller than for k_{-1}. Another indication is that the values for k_{-1} were pH-independent (intercept, Figure 4B), while the values for k_{off} displayed a substantial pH dependence, as described below (Figure 7). The inability to resolve a second phase in NP1/4 is most likely due to similarity in the observed rates for the first and second steps within the limited range of NO concentrations under which the experiment could be performed.

At NO concentrations above 10 μM (at 25 °C), most of the NP2 binding reaction occurred within the dead time of the instrument, so only a fraction of the fast phase could be observed. At 12 °C a larger fraction of the reaction time course was observable, allowing more accurate determinations of the rate constants. At this temperature, k_1 and k_2 for NP2 and NP3 were reduced 2−5-fold (Table 1).

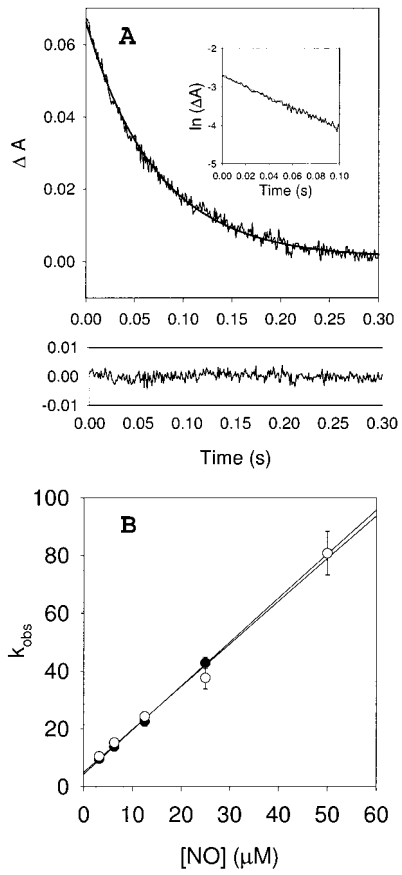

FIGURE 4: NO complex formation with NP1 at pH 5 and pH 8, monitored by stopped-flow mixing. (A) Association of NO (6.25 μM) with NP1 at 25 °C, pH 8.0, and monitored at 400 nm. The data were fit to a single-exponential decay. Plots of ln (ΔA) vs time (inset) and the regression residuals (below) confirm the monophasic rate behavior. (B) Comparison of NP1 kinetics at pH 5.0 (○) and 8.0 (●) in terms of the concentration dependence of k_{obs}, indicating similar association rates occur at the two pHs. Error bars represent SE of at least three replicate experiments.

Table 1: Association Reactions of NO with NP1−4

	pH 5.0		pH 8.0	
	k_1 (μM^{-1} s^{-1})	k_2 (s^{-1})	k_1 (μM^{-1} s^{-1})	k_2 (s^{-1})
NP1[a]	1.5 ± 0.1[b]	nm[c]	1.5 ± 0.1	nm
NP4[a]	2.1	nm	2.3	nm
NP2[a]	22	∼51	33	∼42
NP2[d]	7.3 ± 0.7	∼29	6.8 ± 0.5	∼25
NP3[d]	7.0	∼23	6.7	∼33
metMb (elephant/whale)[e]	$k_1 = 22/0.053$ μM^{-1} s^{-1}			

[a] 25 °C. [b] Where standard errors are included, experiment was replicated at least three times. [c] Not measurable. [d] 12 °C. [e] pH 7.0, 20 °C; taken from Sharma et al. (*11*).

Association reactions for NO with the NPs were also examined by laser flash photolysis. After photolysis of the NP−NO complex, rebinding of NO was observed on the microsecond to millisecond time scale. Under the conditions used, k_{obs} was dependent on the NO concentration, indicating the observed reaction was bimolecular and not geminate (data not shown). At pH 8.0, NP1 and NP4 displayed apparent bimolecular rate constants for NO binding that were similar to those obtained by stopped-flow spectroscopy (not shown).

The amplitude of the flash-induced absorbance change is limited by the quantity of NO leaving the binding pocket during the period of the flash. For NP1−NO, this amplitude decreased by approximately 3-fold at pH 5.0 as compared to pH 8.0, indicating that less NO escapes from the binding pocket after excitation at this pH (Figure 5A,B). Photolysis of the NP2−NO complex was barely detectable at pH 8.0, indicating very little NO escapes the NP2 binding pocket postflash (Figure 5C). These observations correlate with the NO release rate measurements (k_{off}, described below) in that the magnitude of observable photolysis was smallest under conditions where the release rate constant was also smallest.

Histamine Association Reactions. Although the histamine ligand is physically larger than NO, the rate constants for histamine binding at pH 8.0 were similar to or larger than those seen for NO binding (Table 2). The NP2 and NP3 reactions were again biphasic and were analyzed by use of Scheme 2. As with NO binding, the fast-phase rate constant for histamine binding (k_{1H}) was larger for NP2 than for NP1 and NP4, but in this case the difference was only approximately 2-fold greater (Table 2). The slow-phase rate constants for histamine binding to NP2 and NP3 were similar to those found for NO binding (Table 2).

All four NPs displayed smaller rate constants for histamine binding at pH 5.0 than at pH 8.0, presumably due to protonation of the imidazole ring (pK_a 6.9) at pH 5.0, which makes the imidazole nitrogen lone pair electrons inaccessible for binding to the heme iron. It is possible that the charge of the protein binding pocket may also affect histamine binding at lower pH, since ionizable residues participate in histamine binding (*6*).

NO Dissociation Reactions. The first-order rate constants governing dissociation of NO from the unstabilized NP−NO complex (k_{-1}) were estimated from the association reaction data (Figures 3B and 4B) by use of eq 1. As with k_1, the k_{-1} values did not vary with pH for any of the NPs (Figure 4B, Table 3). Overall, the NPs display k_{-1} values that are similar to those of metmyoglobin (Table 1), again suggesting that the formation and dissociation of the initial NP−NO complex is relatively unencumbered.

In contrast, the overall dissociation reactions (represented by k_{off}) were slower than for metmyoglobin, pH-dependent, and biphasic for all four NPs. Values for k_{off} were obtained by a histamine displacement protocol, where excess histamine was added to a solution containing NP−NO and the formation of NP−histamine was monitored spectroscopically (Figure 6; see Materials and Methods for details). At low pH (25 °C), the slower phase rate (k_{off2}) ranged from 0.006 s^{-1} for NP2 to 0.02 s^{-1} for NP1, and the percentage of the overall release as the slower phase ranged from 78% for NP4 to 14% for NP1 (Table 3). The fast-phase rate at pH 5.0 was about 10-fold greater than the slow-phase rate for all four proteins.

NO release was much faster at pH 8 than at pH 5 (Table 3). For NP2 and NP3, the pH 8 values for rate constants k_{off1} and k_{off2} were largely unchanged from their pH 5 values, but the percentage of the overall release as the slower phase decreased to 4% and 20%, respectively, suggesting the fast and slow phases may represent the same events at both pH 8 and 5. Measurements taken at intermediate pH values are consistent with this interpretation (Figure 7). However, for NP1 and NP4, the pH 8 values for k_{off1} and k_{off2} increased by 10−60-fold, but the slower phase amplitude was about 50% of the overall release, indicating that four distinct release

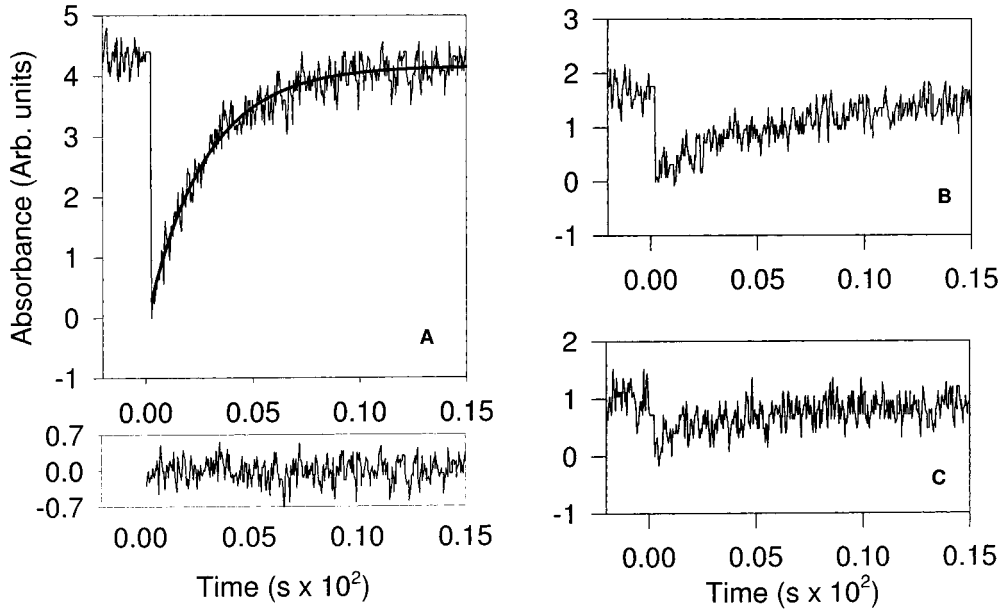

FIGURE 5: Laser flash photolysis of NP−NO complexes monitored at 423 nm. NO and protein concentrations in each case were 1.9 mM and 3.5 μM, respectively. (A) NP1 in 40 mM Tris-HCl, pH 8.0. Data were fit to a single exponential with a rate constant (k_{obs}) of 3680 s^{-1}. (B) NP1 in 40 mM sodium acetate, pH 5.0. (C) NP2 in 40 mM Tris-HCl, pH 8.0.

Table 2: Association Reactions of Histamine with NP1−4

	k_{1H} (μM^{-1} s^{-1}) at pH 5.0	k_{1H} (μM^{-1} s^{-1}) at pH 8.0	k_2 (s^{-1}) at pH 8.0
NP1[a]	0.04 ± 0.01[b]	4.3 ± 0.1	nm[c]
NP4[a]	0.05	4.4	nm
NP2[a]	0.04 ± 0.01	10	∼31
NP2[d]		4.6 ± 0.2	∼12
NP3[e]	0.03	6.8	∼15

[a] 25 °C. [b] Where standard errors are included, experiment was replicated at least three times. [c] Not measurable. [d] 12 °C. [e] 25 °C at pH 6.0 and 12 °C at pH 8.0.

phases, two that are characteristic of the high-pH condition and two that are seen at low pH, occur in these proteins. The rate constants for NP1 at pH 8.0 are similar to those previously reported for NO release after dilution of the recombinant or insect-derived NP1−NO complexes (*16*).

Equilibrium Constants for NP−NO. Dissociation constants governing formation of NP−NO and NP′−NO, as well as the overall dissociation constant, were calculated where possible from the kinetic data in Tables 1 and 3 (Table 4). The overall dissociation constants were also directly measured for NP1, NP2, and NP4 (Table 4), although the ligand affinity was too high with NP2 at pH 5.0 for an accurate measurement to be made (see Materials and Methods). Both measured and calculated values for NP2 at pH 8.0 were obtained in this way and differed by only 3-fold, suggesting that no major errors were introduced by the approximations used in the kinetic measurements and also that no major kinetic phases were missed in the analyses. Likewise, K_d can also be estimated as k_1/k_{off}, and these values differed from the measured K_d values by only 1−5-fold (Table 4).

The values obtained for K_{-1} were similar in all three proteins at both pHs examined (∼3 μM) and similar to that for elephant metmyoglobin (1.8 μM). This is consistent with formation of an initial complex that does not require displacement of a stabilized distal ligand. In contrast, sperm whale metmyoglobin has a stabilized water molecule in the sixth heme ligation position that must be dislodged for NO complex formation, which leads to a 40-fold increase in K_d over that for elephant metmyoglobin, where this water is not stabilized (*11*).

For NP2 at 25 °C, K_{-2} could be estimated from the ratio of k_{-2}/k_2, where k_{-2} was obtained from eq 4 by use of an amplitude-weighted average of the two k_{off} values. The derived values, 0.0007 and 0.007 at pH 5 and 8, respectively, are consistent with a favorable stabilization process, such as the conformational change seen in the NP4−NO crystal structure. Destabilization of the NP′−NO complex, to give NP−NO, also appears to be the only pH-sensitive step in the formation and release of NO by the NPs.

Measurements of K_d for NP4−NO at pH 6.0 and 7.0 were intermediate between the values obtained at pH 5.0 and 8.0. A fit of these data to a titration function were consistent with a two-state equilibrium between low-pH and high-pH NP forms, governed by a single ionizable group having a pK_a of 6.5 (Figure 8). However, the participation of multiple residues with approximately equal pK_a values cannot yet be ruled out. These pH dependencies are similar to those reported for a salivary gland homogenate containing a mixture of all four NPs (*4*).

Dissociation Rate and Equilibrium Constants for NP-Histamine. Where the stopped-flow data for histamine binding to the NPs were sufficiently robust, k_{-1H} could be estimated from eq 1 (Materials and Methods), yielding values similar to k_{-1} for NO release (Table 5). Spectral K_d values for histamine were also measured for all four proteins at pH 8.0 and found to be ∼10 nM in all cases (Table 5), in agreement with previous reports for insect-derived and recombinant NP1 (*5*, *6*). The values are 50-fold smaller than for NO binding to NP1 and NP4 at pH 8.0, and about the same as for NO binding to NP2. The presence of a second stabilizing phase for histamine binding is again indicated by comparison of K_{-1H} ($= k_{-1H}/k_{1H}$) with the directly measured K_d, which is about 100-fold smaller. In this case, stabilization

Table 3: Dissociation Reactions of NO with NP1−4

	pH 5.0				pH 8.0			
	k_{-1}[a] (s^{-1})	k_{off1}[b] (s^{-1})	k_{off2}[c] (s^{-1})	fast[d] (%)	k_{-1}[a] (s^{-1})	k_{off1}[b] (s^{-1})	k_{off2}[c] (s^{-1})	fast[d] (%)
NP1	5 ± 2	0.20 ± 0.01	0.02 ± 0.001	86	4.3 ± 0.7	2.2 ± 0.1	0.6 ± 0.02	50
NP4	3.4	0.14 ± 0.01	0.01 ± 0.002	22	6.3	2.6 ± 0.1	0.6 ± 0.01	39
NP2	52. 27 ± 4[e]	0.05 ± 0.01	0.006 ± 0.001	30	32 27 ± 6[e]	0.12 ± 0.01	0.01 ± 0.002	96
NP3	16[e]	0.05 ± 0.01	0.005 ± 0.001	23	30[e]	0.08 ± 0.01	0.01 ± 0.001	80
			metMb (elephant/whale)[f]		k_{off} = 40/14 s^{-1}			

[a] Intercept from stopped-flow association data. [b] Fast phase, histidine displacement data. [c] Slow phase, histidine displacement data. [d] Percentage release in fast phase. [e] 12 °C, all others at 25 °C. [f] pH 7.0, 20 °C; taken from Sharma et al. (*11*).

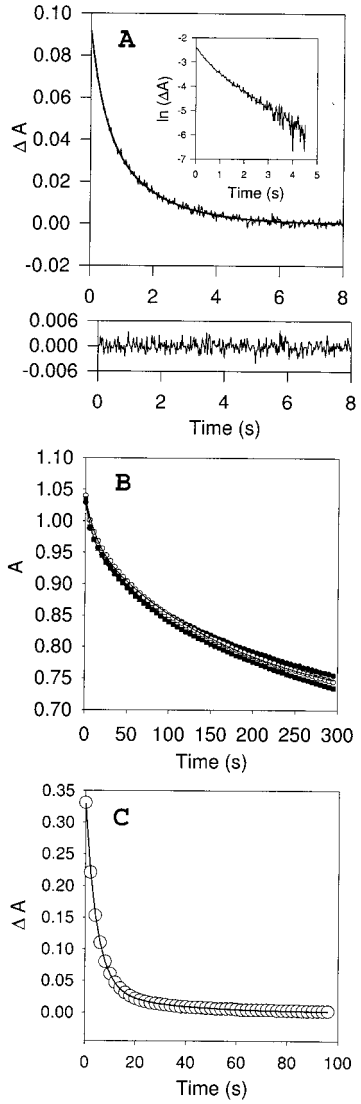

FIGURE 6: Histamine displacement of NO bound to NP1 and NP4. (A) Mixing of NP4−NO (10 μM in 40 mM Tris-HCl, pH 8.0) with histamine (4 mM, same buffer) in a stopped-flow device (25 °C), with monitoring at 423 nm. The curve and error analysis from fitting to a double-exponential decay are shown. The inset shows a plot of ln (ΔA) vs time for the same data, confirming the presence of two phases. (B) Mixing of NP4−NO (10 μM in 40 mM sodium acetate, pH 5.0) with histamine (1, 5, and 10 mM, same buffer) in a sealed cuvette (25 °C), monitored in a spectrophotometer at 423 nm. Essentially identical biphasic release rates were observed at all three histamine concentrations, as illustrated. (C) Mixing of NP1−NO with 10 mM histamine, pH 5.0, as described in panel B except with ΔA plotted.

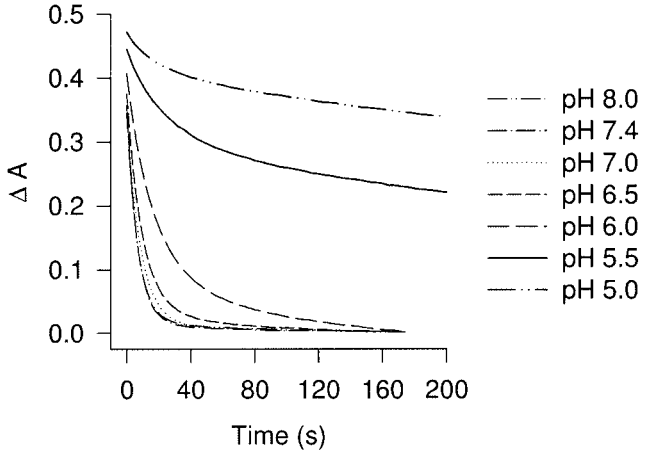

FIGURE 7: pH dependence of NO release from NP2. Shown are the double-exponential decay curves for histamine replacement undertaken as described in Figure 6. The values for k_{off1} and k_{off2} were similar at all pHs, but the amplitude of the slow phase become greater, and the fast phase lesser, as the pH decreased. Buffers used: Tris-HCl, 40 mM, pH 8.0; sodium phosphate, 40 mM, pH 7.4; sodium phosphate, 40 mM, pH 7.0; sodium citrate, 40 mM, pH 6.5; sodium citrate, 40 mM, pH 6.0; sodium acetate, 40 mM, pH 5.5; sodium acetate, 40 mM, pH 5.0.

may be due to a slight ligand-induced ordering of the binding pocket loops, and the formation of four additional hydrogen bonds between the protein and ligand, as shown in the structure of NP1−histamine (*6*).

Electrochemical Studies: Spectral Changes with pH and Applied Potential. We have measured the reduction potentials and spectral properties of all four NPs to further understand the stability of the ferric nitrosyl complex in these proteins. As explained in the introduction, stabilizing the ferric form of the protein is critical for the NPs to function as NO transporters. These proteins also provide an opportunity for examining factors related to ferrous nitrosyl complexes, such as occurs in soluble guanylate cyclase (sGC), where NO binding to ferrous heme stimulates cyclase activity and the formation of cGMP, the intracellular second messenger that, for example, leads to vasodilation (reviewed in ref *24*).

Optical spectra of the ferric and ferrous NP3−NO complexes at pH 5.5 and 7.5, as a function of applied potential, are shown in Figure 9. The UV−visible spectra of all NP−NO complexes in their oxidized and reduced forms are similar to those of $NP1^{III}$−NO and $NP1^{II}$−NO (*12*), as well as to metmyoglobin−NO and myoglobin−NO (*14*, *25*). For the NP1/4−NO complexes, the Soret bands shift from 419 to 416 nm upon reduction to the ferrous state and do not change over the pH 5.5−7.5 range. In contrast, for the NP2/3−NO complexes, the Soret bands shift from 421 and 413 nm at pH 8.0 and 7.5, but at pH 5.5, the reduced form has its Soret band at 395 nm (Figure 9A), presumably

Table 4: Equilibrium Constants for NO Dissociation of 25 °C from NP1, 2, and 4

	pH 5.0 ($\times 10^{-6}$)					pH 8.0 ($\times 10-6$)				
	K_{-1}[a]	K_{-2}[b]	$K_{-1}K_{-2}$[c]	k_{off}/k_1[d]	K_d[e]	K_{-1}[a]	K_{-2}[b]	$K_{-1}K_{-2}$[c]	k_{off}/k_1[d]	K_d[e]
NP1	5.4			0.11	0.12 ± 0.02	2.8			0.9	0.85 ± 0.06
NP4	1.6			0.02	0.05 ± 0.003	2.7			0.6	0.54 ± 0.02
NP2	2.4	700	0.002	0.001	−	1.0	6600	0.007	0.004	0.02 ± 0.004
				metMb (elephant/whale)[f]		$K_d = 1.8/264\ \mu M$				

[a] k_{-1}/k_1 from Tables 1 and 3. [b] k_{-2}/k_2, where k_2 was from Table 1 and k_{-2} was derived from eq 4, using a linear combination of fast and slow k_{off} components in Table 3. [c] Overall dissociation constant (micromolar) estimated from all four rate constants ($K_{-1}K_{-2}$). [d] Overall dissociation constant (micromolar) estimated from two limiting rate constants (k_{off}/k_1). [e] Direct measurement of the dissociation constant. [f] Ratio of k_{off}/k_{on}; taken from Sharma et al. (*11*).

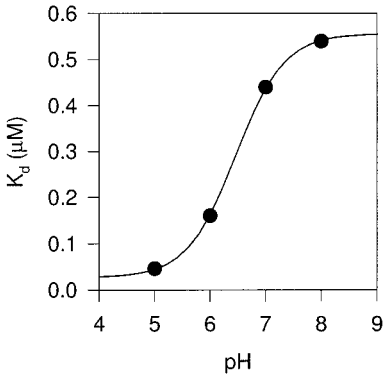

FIGURE 8: Plot of K_d vs pH for NP4−NO. The data are fit to the equation for a titration curve, eq 6, yielding an apparent pK_a of 6.5.

Table 5: Rate and Equilibrium Constants for Histamine Dissociation from NP1−4

	pH 5.0		pH 8.0		
	k_{-1H} (s^{-1})	K_{-1H} (μM)	k_{-1H} (s^{-1})	K_{-1H} (μM)	K_{dH} (μM)
NP1[a]	1.3 ± 0.4	32			0.011 ± 0.008
NP4[a]	2.2	44			0.010 ± 0.001
NP2[a]	1.4 ± 0.7	35	16	1.6	0.009 ± 0.001
NP2[b]			14 ± 5	2.9	
NP3[c]	1.0	33	13	1.9	0.018 ± 0.003

[a] 25 °C. [b] 12 °C. [c] 25 °C at pH 5.0 and 12 °C at pH 8.0.

due to breakage of the proximal histidine−iron bond. Both the wavelength maximum and shape of the 395 nm Soret band are typical of five-coordinate heme−NO centers, such as occurs in the sGC nitrosyl complex, where breakage of the proximal histidine bond is thought to initiate a conformational change that increases cyclase activity (*24*). At the intermediate pH values 6.5 and 7.0, the redox behavior of NP2−NO was found to be nonisosbestic, which is typical for the presence of more than two absorbing species in the solution. Isosbestic behavior is observed at all other pHs for all of the nitrophorins (see, for example, Figure 9B). Thus, the proximal histidine apparently dissociates in the ferrous NP2/3 nitrosyl complexes at pHs below ~7. The structural basis for this difference between NP1/4 and NP2/3 is not yet clear: the NP2−ammonia complex structure has a proximal-side heme environment that looks nearly identical to that of the NP1/4 ammonia complexes (*26*).

The spectral changes were reversible in all cases over many cycles of positive and negative applied potential, as positive as +600 mV vs Ag/AgCl (+805 mV vs NHE), and the ferric forms of the nitrophorin−NO complexes have the higher extinction coefficients and sharper Soret and α, β

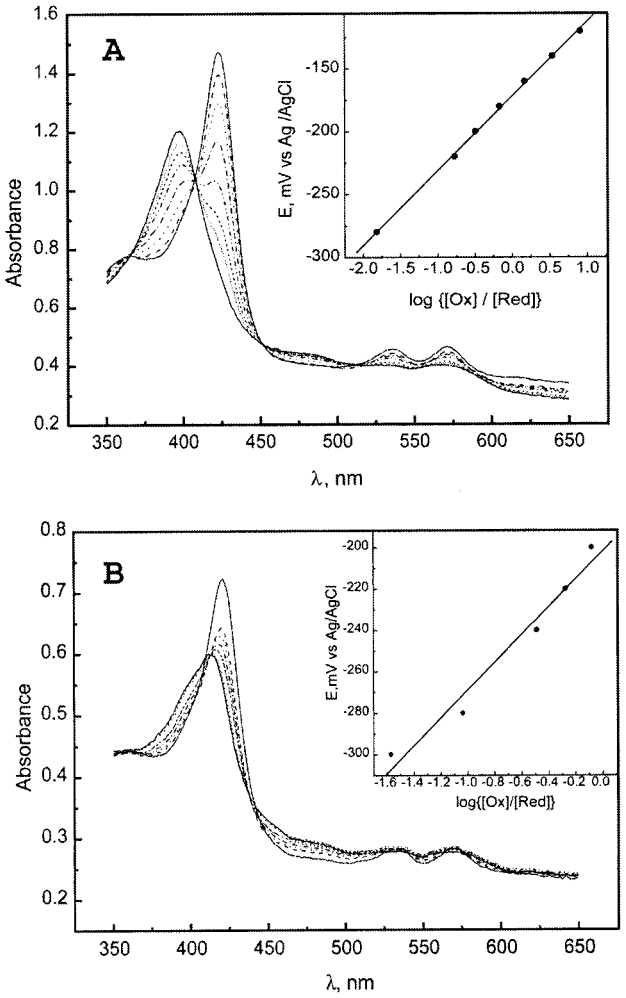

FIGURE 9: (A) UV−visible spectra of NP3−NO at pH 5.5 as a function of applied potential. In order of decreasing Soret band heights (for A): 0, −120, −140, −160, −180, −200, −220, −280 mV vs Ag/AgCl, respectively (add 205 mV for potential vs NHE). Inset: Nernst plot of the spectroelectrochemical data (eq 7, Materials and Methods), showing the expected linear behavior. (B) UV−visible spectra of NP3−NO at pH 7.5 as a function of applied potential, in order of decreasing Soret band heights at 428 nm (for B): 0, −200, −240, −260, −280, −300, −320 mV vs Ag/AgCl, respectively. Inset: Nernst plot of the spectroelectrochemical data. The −260 and −320 mV data points yielded unreasonable values of log[ox]/[red] and were thus not included in the Nernst plot.

bands. As reported for NP1−NO (*12*), at pH 7.5, application of a positive potential of up to +600 mV causes the Soret band to shift to 403 nm, indicating that the oxidized form, $NP4^{III}$−NO, readily loses NO when an oxidizing potential is applied, probably due to oxidation of free NO as it dissociates. This result is consistent with the ~20-fold larger

Table 6: Reduction Potentials[a] and Derived Ratios of Ferrous and Ferric Dissociation Constants

	pH	NP1	NP4	NP2	NP3
			Aqua Complexes		
$E°$ (mV)	5.5	-274 ± 2[b]	-259 ± 2	-287 ± 5	-321 ± 5
	7.5	-303 ± 4[b]	-278 ± 4	-310 ± 5	-335 ± 3
			NO Complexes		
$E°$ (mV)	5.5	$+154 \pm 5$[b]	$+94 \pm 5$	$+49 \pm 3$	$+33 \pm 4$
	7.5	$+127 \pm 4$[b]	[c]	$+8 \pm 3$	$+3 \pm 5$
K_d^{III}/K_d^{II} [d]	5.5	1.6×10^7	8.5×10^5	4.4×10^5	8.9×10^5
	7.5	1.7×10^7		2.2×10^5	4.8×10^5
			Histamine Complexes		
$E°$ (mV)	5.5	-339 ± 2	-393 ± 2	-410 ± 3	-353 ± 8
	7.5	-403 ± 1	-404 ± 1	-452 ± 4	-445 ± 3
K_d^{III}/K_d^{II} [d]	5.5	8.1×10^{-2}	5.6×10^{-3}	8.6×10^{-3}	2.9×10^{-1}
	7.5	2.1×10^{-2}	7.6×10^{-3}	4.1×10^{-3}	1.4×10^{-2}

[a] All potentials ($E°$) are expressed in millivolts vs NHE (+205 mV with respect to the Ag/AgCl electrode used in the spectroelectrochemical titrations). For comparison, the value for horse heart metmyogobin is ~0 mV at all pHs for the unligated molecule but could not be measured for the NO complex (*12*). [b] From ref *12*. [c] Could not be measured (see text). [d] Calculated from eq 8.

values of k_{off} for NP1 and NP4 at higher pH than at lower pH (Table 3). The loss of NO upon oxidation of the protein−NO complex to the Fe(III) state is rapid enough that it was not possible to measure the reduction potential of NP4^{III}−NO at pH 7.5.

The optical spectra of the ferric and ferrous forms of NP2−4 in the absence of NO over the pH range of 5.5−7.5 show the more typically expected changes in Soret band maximum observed previously for NP1 (*12*). The high-spin NP^{III} species have their Soret band maxima at 402−403 nm, while the high-spin NP^{II} have their Soret band maxima at 430 nm at pH 5.5 for NP1 and NP4 and 417−418 nm for NP2 and NP3. In all cases the α, β bands are quite broad and of low extinction. In the presence of histamine, the Soret band maximum of the Fe(III) form of the NPs was at 410 nm, and upon reduction, the band shifted to 424 nm.

Reduction Potentials of the NPs and Their NO and Histamine Complexes. By use of the spectral data described above, Nernst plots such as those shown in the inserts of Figure 9 were constructed, and the midpoint potentials of the NPs and their NO and histamine complexes were calculated (Table 6). In all cases, the slopes of the Nernst plots were 60 ± 2 mV, indicating a well-behaved electrochemical titration. The reduction potentials of all four NPs in the absence of NO or histamine are within 20−40 mV of each other. The reduction potentials of their NO complexes, however, differ significantly from each other. For example, the reduction potential of NP4−NO is about 350 mV more positive than that of NP4 in the absence of NO, as compared to a 430 mV shift for NP1 upon binding NO. In contrast, the histamine complexes have much more negative reduction potentials, by 100−150 mV at pH 7.5, than the NPs in the absence of added ligands. These more negative potentials are indicative of the fact that the Fe(III) histamine complexes are more stable than their corresponding Fe(II) complexes, unlike with the nitrosyl complexes, where the Fe(II) complexes are more stable.

The ratio of the ferric and ferrous ligand dissociation constants were calculated by use of eq 8 (Materials and Methods). As can be seen in Table 6, the K_d values for the Fe(III)−NO complexes are 10^5−10^7-fold larger than those for the respective Fe(II)−NO complexes, with NP1 showing the largest increase in K_d when the metal is oxidized. The ratio K_d^{III}/K_d^{II} either remains constant or decreases by about a factor of 2 as the pH is increased, which, combined with the fact that K_d^{III} increases with pH (Table 4), means that K_d^{II} also increases with pH. Combined with the K_d^{III} values of Table 4, the NP^{II}−NO dissociation constants are found to be extremely small: only 5−90 *femtomolar*. In contrast, for the histamine complexes, it is K_d^{III} that is smallest, and the Fe(III)-histamine complexes are 3−244-fold more stable than the Fe(II) complexes. Thus, the Fe(III) oxidation state of the NPs favors the dissociation of NO and the binding of histamine, whereas the Fe(II) oxidation state favors just the opposite. Clearly, the NPs have evolved a pocket that stabilizes ferric heme in order to facilitate NO transport and dissociation and histamine binding.

DISCUSSION

In the foregoing, we describe kinetic, equilibrium, and electrochemical analyses for ligand binding to all four nitrophorins. The results are consistent with two-step mechanisms for binding and release of NO and histamine for all four NPs (Scheme 4). They also confirm that all four NPs are stabilized in their ferriheme states when unligated (by ~300 mV or 7 kcal mol^{-1} with respect to metmyoglobin) and when in their NO complexes (Table 6). The initial NP binding reaction with NO, k_1, is fast (1.5−33 μM^{-1} s^{-1}, Table 1) and consistent with an unhindered path to the distal heme binding site. The second NO binding step, which is most likely due to conformational changes in loops A−B and G−H (Figure 1), is relatively slow for an intramolecular event (k_2 ~50 s^{-1} for NP2 at 25 °C). Similarly, release of NO is characterized by a very slow step (k_{-2}, 0.02−1.4 s^{-1}, Table 3), which we hypothesize to require disordering of the distal pocket loops, and a faster step (k_{-1}, 3−52 s^{-1}, Table 3) that likely relates to thermal bond breakage and unhindered escape from the distal pocket. Overall NO dissociation constants calculated from the combination of rate constants agree well with directly measured values and lie in the range of 1−850 nM (Table 4). This suggests no major kinetic steps are missing from Scheme 2 and no substantial errors arose from the assumptions inherent in the experimental protocol used. The kinetic values vary among the NPs in that values for NO off rates are 2−12-fold smaller and on rates are 10−22-fold larger for NP2/3 than for NP1/4, leading to dissociation constants that are ~30−100-fold smaller. These trends reflect the greater sequence identity in the NP1/4 and NP2/3 pairs.

The NPs perform different functions depending on their physical location. In the insect salivary gland, the proteins store NO in a protected state, while in the tissue of the host, the proteins release NO and sequester histamine. To carry out these mutually exclusive functions, the protein senses the increase in pH that occurs on moving from the saliva (pH ~ 5) to the host (pH ~ 7.2). As expected (*4*, *16*), the recombinant proteins display a 7−11-fold increase in K_d as the pH increases. The only pH-sensitive step is the slower release step, k_{-2}, which also increases (from 6- to 33-fold). The reduction potentials are largely pH-insensitive, suggesting the change in NO affinity on raising the pH is due to something other than a change in the NO−heme bond

characteristics, such as a change in the dynamics of the distal pocket loop. The mechanism by which the ferric state is stabilized at all pHs is not yet known but may be electrostatic in nature, through the several acidic amino acids in the distal pocket vicinity, as discussed in detail elsewhere (*12*), or may result from the severe heme ruffling that occurs in these proteins (*6*, *9*, *18*, *26*).

Comparison with Myoglobin. It is instructive to compare our findings with the large body of data available for metmyoglobin, which bears many similarities to the NPs. Both are relatively small soluble proteins that contain a b-type high-spin Fe(III) heme. In each, a histidine residue from the protein acts as the proximal ligand. Yet NPs show a higher affinity for NO (Table 4), a slower release rate (Table 3), and a resistance to NO-mediated autoreduction (Table 6) relative to metmyoglobins, particularly at pH 5.0, where k_{off} values for the NPs are 82−2000-fold smaller than for the metmyoglobins (kinetic values for metmyoglobins are from ref *11*).

The bimolecular rate constants for NO binding with NPs range from 1.5 to 33 μM^{-1} s^{-1} (Table 1), similar to that for elephant metmyoglobin (22 μM^{-1} s^{-1}) but several hundred-fold larger than that for sperm whale metmyoglobin (0.053 μM^{-1} s^{-1}). The small value for sperm whale metmyoglobin is thought to arise from an aqua complex that is stabilized through a hydrogen bond to the distal histidine, which leads to a slow displacement reaction. In elephant metmyoglobin, a distally coordinated water molecule must also be displaced, but it is apparently not stabilized to the degree seen in sperm whale metmyoglobin (*11*, *23*). Likewise, a distally coordinated ligand is also present in the structures of NP1, NP2, and NP4 and has been identified as either ammonia or water, depending on the crystallization conditions (*6*, *9*, *26*). This ligand is not stabilized by direct interaction with the protein and appears to be only weakly coordinated, a fact that is apparently reflected in the faster association kinetics relative to sperm whale metmyoglobin.

In addition to displacement of a coordinated ligand, accessibility to the heme-binding pocket from the solvent is an important consideration for ligand binding reactions. In sperm whale myoglobin, a movement of the distal histidine side chain is necessary for displacement of distal pocket water. This would include both coordinated water in metmyoglobin and noncoordinated water in deoxymyoglobin (*11*, *27*). The crystal structures of NO-free nitrophorins show that although water must be displaced from the distal pocket, no movement of protein residues is required for ligand entry or water exit. The similarity in the association kinetics for NO and histamine suggest that steric hindrance to ligand entry is not rate-limiting, since a large ligand (histamine) and a small ligand (NO) can enter the binding pocket at similar rates. In contrast, imidazole binding to wild-type and mutant forms of sperm whale myoglobin suggest steric hindrance through the distal histidine plays a limiting role in association reactions (*28*). The larger association rate constants for both NO and histamine binding in NP2 and NP3 may be due to a greater ease of solvent displacement from these proteins. In NP1/4, the side chains of Lys 38, Lys 125, Asp 34, and one of the heme propionate groups partially block entry to the distal pocket, and polar residue Thr 121 is at the back of the distal pocket. In the NP2 crystal structure, the side chains and propionate groups at the front of the distal pocket are arranged differently, creating a more open entry to the binding pocket, and the residue corresponding to Thr 121 becomes a nonpolar isoleucine (Ile 120; *26*). Taken together, these factors may lead to a more favorable path for the exit of solvent molecules in NP2/3 (Figure 10).

The values for $k_{-1,}$ the faster, non-pH-dependent NO dissociation rate constant, range between 3 and 52 s^{-1} for the NPs and are again similar to the values displayed by the metmyoglobins (Table 3). We hypothesize that this faster rate represents dissociation from the open NP distal pocket, which occurs at a similar rate for all NPs and does not vary with pH. For the globins, ligand dissociation is thought to be limited only by the rate of thermal Fe−L bond breakage (*29*), and the same may well be true of k_{-1} for the NPs.

Multiphasic Kinetics and Conformational Changes. Unlike the globins, the NPs display additional, slower binding and dissociation phases. This multiphasic behavior suggests that the NPs are not conformationally homogeneous and that relatively slow (milliseconds to seconds) interconversions between conformers occur, leading to stabilized complexes. The most likely candidate for this is the NO-induced conformational change described for NP4 in the introduction (Figure 1); however, the mechanism by which the closed conformer protects and stabilizes the complex is not yet clear. Most likely, the conversion of the distal pocket to an essentially nonpolar environment plays a central role, since NO is 70 times more soluble in nonpolar solvents than polar solvents (*30*, *31*). NO appears to have freedom for limited diffusion about the distal pocket, based on the appearance of multiple orientations for the molecule in the crystal structure (*18*), but exchange with the aqueous solvent is apparently hindered, despite the fact that the loops filling the distal pocket have higher mobility on average than the rest of the protein, based on crystallographic temperature factors. That the loop dynamics do indeed give rise to the slower on and off phases seems clear though, since preliminary measurements with the NP4 mutants D30N and D30A display k_{off} values that are significantly larger than for the wild-type protein. Asp 30 lies in loop A−B (between β-strands A and B) and becomes buried in the closed conformation (Figure 1).

Additional insight may come from NMR studies of the heme resonances of the imidazole complex of NP1, where a chemical exchange between two sets of resonances of similar chemical shift has been uncovered (Shokhireva and Walker, unpublished results.) One set is nearly unobservable in the 1D spectrum yet exhibits very strong chemical exchange cross-peaks in NOESY/EXSY spectra. It is clear that the multiple resonances involve some change in conformation of one or more protein side chains, such as those of the A−B loop, which are quite fluxional (Figure 1). Preliminary analysis of the diagonal and cross-peak intensities in these 2D spectra in terms of a two-site chemical exchange process, X ↔ Y, where Y represents the species giving rise to the small peak, yields rate constants of the order of $k_{YX} \sim 70-90$ s^{-1} and $k_{XY} \sim 7-10$ s^{-1} and $K_{eq} \sim 0.1$ at pH 7.0, 30 °C (F. A. Walker, T. Kh. Shokhirev and N. V. Shokhireva, unpublished results). Further investigation is underway to determine whether the rate process observed by NMR spectroscopy is related to the slow step (k_2) observed in the stopped flow kinetics for NO binding.

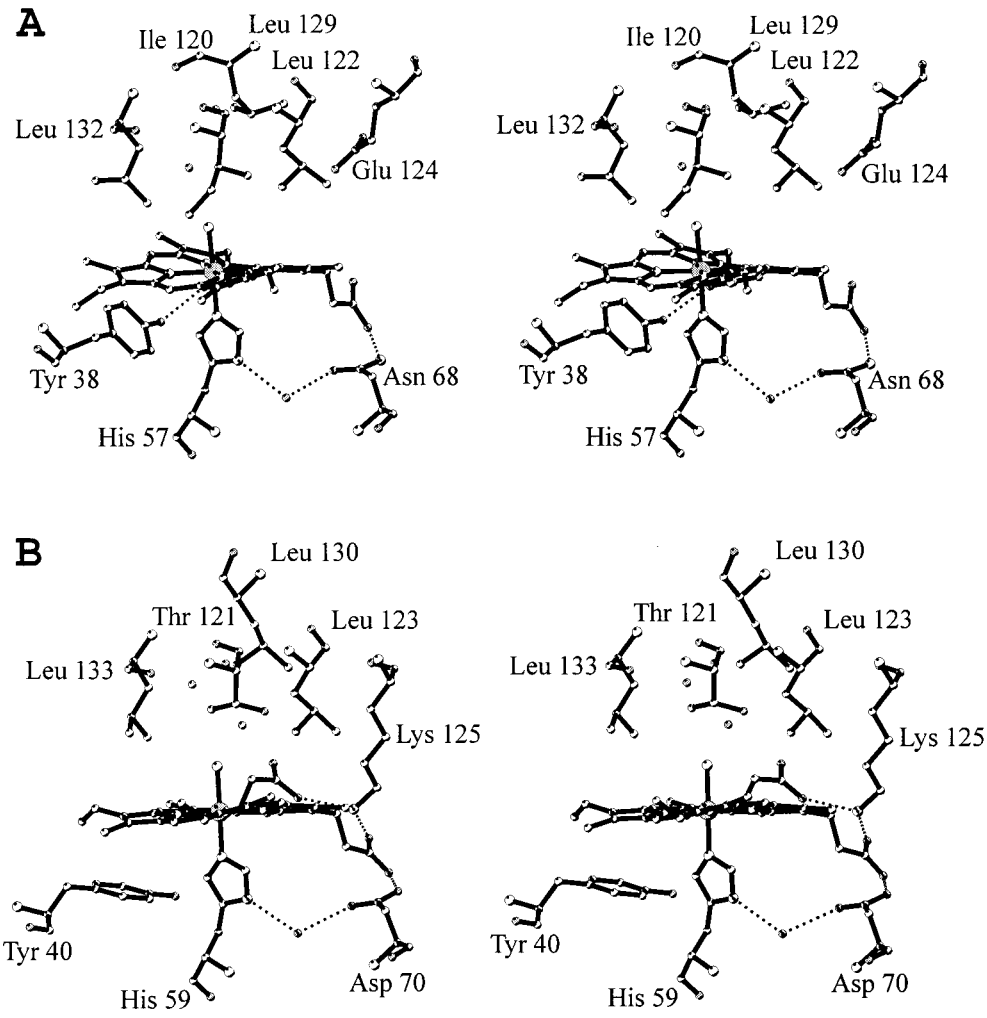

FIGURE 10: Stereoview of the NP2 and NP4 distal pockets in their open conformations. (A) NP2; (B) NP4.

The NPs have a second kinetic phase for both binding and release of NO that differs somewhat between NP1/4 and NP2/3 but results in tighter binding for all four proteins. For binding by NP2/3, double-exponential binding kinetics are clearly observed (Figure 3), with the second phase displaying a rate that does not have a linear NO concentration dependence, consistent with a sequential mechanism where NP−NO converts to NP′−NO (Scheme 4). Kaneko et al. (*17*) have also observed this for NP2, although the rate constant for the fast binding phase is smaller in their hands. The second binding phase could not be directly measured for NP1/4, but its occurrence is clearly indicated by the fact that the k_{-1} and K_{-1} values for NO dissociation are larger than k_{off} and K_d, respectively. This stabilization is small at pH 8.0 but increases by 32−45-fold for NP1/4 and by at least several hundredfold for NP2/3 as the pH is lowered to 5.0 (Table 4).

The observed biphasic kinetics for NO release also differ between NP1/4 and NP2/3. With NP2, the two phases can be attributed to the low- and high-pH forms of the protein since the values for k_{off1} and k_{off2} were similar at all pHs, but the slow-phase amplitude is small at high pH and increases as the pH is lowered (Figure 7, Table 3). However, NP1 and NP4 show two phases with approximately equal amplitude at pH 8.0, suggesting the possibility of multiple conformations at this pH. A similar observation has been made with the H64M (position E7) mutant of sperm whale myoglobin (*32*). In this case, ligand release follows biphasic kinetics, apparently due to a slow interconversion between conformers of the methionine side chain (*32*). The structure of the ligand-binding pocket is also known to influence the overall release rate for NO from myoglobin. A bulky hydrophobic residue at position B10 (residue 29) leads to higher rates of geminate recombination, and consequently, a smaller release rate (*33*). Additional studies have further demonstrated the important role of distal pocket structure in geminate recombination (*29*, *34*−*36*). Thus, it is possible that for NP1/4, there are two distal pocket environments that give rise to differing release rates and that these different environments also change as a function of pH. The multiple NO conformations found in the structure of the NP4−NO complex (*18*) provide one possible explanation for the multiple release rates.

The results of flash photolysis experiments with the NP−NO complexes also support a model in which the degree of stabilization of the complex varies among NP forms and with pH. The relative amplitudes of the transients shown in Figure 5 correlate with the relative values of the release rate constants. Conditions giving a smaller NO release rate constant also give a smaller value for the yield of photoproduct. If these differences were simply due to differing Fe−NO bond strengths, then the reduction potentials would

be expected to follow a similar trend, but such is not the case (Table 6). An alternative explanation for these results is that the reactivity of the iron is approximately equal in each case, but escape from the ligand-binding pocket is hindered to a larger degree in NP2 at pH 8.0 and NP1 at pH 5.0. This model would require a hindrance to escape from the binding pocket that increases the proportion of NO rebinding to the iron atom after photolytic cleavage, relative to the proportion that escapes from the binding pocket. To determine whether photolytic bond cleavage or escape from the binding pocket is rate-limiting in these studies will require measurements of geminate recombination by nanosecond or picosecond laser photolysis (*33*).

More broadly considered, conformational changes in the NPs serve as an alternative mechanism to that of the globins for heme-based signaling by gaseous ligands. In hemoglobin, a change in the heme geometry is the initial event that gives rise to allosteric regulation. Similar schemes have also been proposed for the oxygen sensor FixL, which is inactivated through oxygen binding to a heme center (*37*), and for sGC, which is activated through NO binding to a heme center (*24*). In contrast, the key event with the NPs is apparently the sensing of a distal pocket change in polarity rather than a difference in heme geometry between the nitrosyl and aqua complexes (*18*).

Histamine and the Mechanism of Nitric Oxide Delivery. Although heme proteins commonly bind nitrogen heterocycles with reasonably high affinity, the binding of histamine by the NPs is clearly an adaptive feature, since it involves four specific hydrogen bonds with the protein (*6*) that lead to a complex with $K_d \approx 10$ nM (Table 5) and gives rise to an antihistaminic activity that most likely reduces local inflammation, permitting the insect to feed undisturbed (*5*). The histamine complex of NP1 also reveals substrate-mediated ordering of loops A−B and G−H (*6*), which, although less dramatic than those seen in the NP4−NO complex, still apparently result in biphasic kinetics (Tables 2 and 5). A similar strategy is used by the tick, another slow blood-feeding insect (*38*). Interestingly, the tick also uses a lipocalin-like protein to bind histamine but does so without heme. In the NPs, the use of ferric heme for both NO and histamine binding is chemically advantageous, since binding of histamine is stronger to ferriheme than ferroheme (Table 6), but the Fe^{III}−NO bond is weak enough to allow rapid release ($K_{-1} \approx 3$ μM, Table 4).

The role of histamine in displacing NO or, more precisely, in inhibiting NO rebinding after release is supported by the present studies. At pH 8.0, histamine binds with a bimolecular rate constant that is quite similar to that seen with NO. A relatively small excess of histamine would efficiently inhibit the rebinding of NO with the NP protein, especially in the vicinity of the bite, where the NP concentration would be highest. Also, the release rate for histamine is slower than the slowest rate seen for NO release at pH 8.0, effectively blocking the NO binding site and preventing rebinding (Tables 3 and 5). Thus, the kinetic data suggest that, in addition to antihistaminic activity, histamine binding also functions to increase the efficiency of NO release by rapidly replacing it in the ligand-binding pocket.

Multiplicity of Nitrophorin Forms. Why are four NP forms present in the saliva instead of only one? Most likely, the answer lies in the functional diversity that can be built into a four-member family. The proteins share only 38% overall sequence identity but fall into two functional groups, NP1/4 and NP2/3. NP1 is reported to be the most abundant of the four proteins in *R. prolixus* saliva, followed by NP2, NP3, and NP4, but the quantity of NP1/4 is about equal to that of NP2/3 (*39*). The present studies indicate the differences among the NP−NO release rates are sufficiently large to allow additional properties to emerge. By use of the release rate constants described herein, it appears the multiple NP forms allow both a rapid burst of NO release after injection into the host, and a sustained release for many seconds. Under conditions of large histamine excess at pH 8.0, NP1 and NP4 release NO with a half-time of 0.3−1 s, while NP2 and NP3 release with a half-time of 7 s. The two release rates of the mixture would therefore presumably prolong the duration of the NO signal and increase the radial extent of the signal around the point of the bite, while still allowing an instantaneous signal to occur.

ACKNOWLEDGMENT

We thank Drs. Michael Cusanovich and John Fitch for help with the stopped-flow experiments, Drs. Gordon Tollin and James Hazzard for help with the flash-photolysis experiments, and Wallace Clark for N-terminal sequence and mass spectrometry analyses.

REFERENCES

1. Kirchhoff, L. V. (1993) *N. Engl. J. Med. 329*, 639−644.
2. Law, J., Ribeiro, J. M. C., and Wells, M. (1992) *Annu. Rev. Biochem. 61*, 87−111.
3. Montfort, W. R., Weichsel, A., and Andersen, J. F. (2000) *Biochim. Biophys. Acta* (in press).
4. Ribeiro, J. M. C., Hazzard, J. M. H., Nussenzveig, R. H., Champagne, D. E., and Walker, F. A. (1993) *Science 260*, 539−541.
5. Ribeiro, J. M. C., and Walker, F. A. (1994) *J. Exp. Med. 180*, 2251−2257.
6. Weichsel, A., Andersen, J. F., Champagne, D. E., Walker, F. A., and Montfort, W. R. (1998) *Nat. Struct. Biol. 5*, 304−309.
7. Ribeiro, J. M. C., Schneider, M., and Guimaraes, J. A. (1995) *Biochem. J. 308*, 243−249.
8. Sun, J., Yamaguchi, M., Yuda, M., Miura, K., Takeya, H., Hirai, M., Matsuoka, H., Ando, K., Watanabe, T., Suzuki, K., and Chinzei, Y. (1996) *Thromb. Hemostasis 75*, 573−577.
9. Andersen, J. F., Weichsel, A., Balfour, C. A., Champagne, D. E., and Montfort, W. R. (1998) *Structure 6*, 1315−27.
10. Walker, F. A., Ribeiro., J. M. C., and Montfort, W. R. (1999) in *Metals in Biological Systems, Vol. 36: Interrelations between Free Radicals and Metal Ions in Life Processes* (Sigel, A., and Sigel, H., Eds.) pp 621−663, Macel Dekker, New York.
11. Sharma, V. S., Traylor, T. G., Gardiner, R., and Mizukami, H. (1987) *Biochemistry 26*, 3837−3843.
12. Ding, X. D., Weichsel, A., Andersen, J. F., Shokhireva, T. K., Balfour, C., Pierik, A. J., Averill, B. A., Montfort, W. R., and Walker., F. A. (1999) *J. Am. Chem. Soc. 121*, 128−138.
13. Sharma, V. S., Isaacson, R. A., John, M. E., Waterman, M. R., and Chevion, M. (1983) *Biochemsitry 22*, 3897−3902.
14. Addison, A. W., and Stephanos, J. J. (1986) *Biochemistry 25*, 4104−4113.
15. Hoshino, M., Maeda, M., Konishi, R., Seki, H., and Ford, P. C. (1996) *J. Am. Chem. Soc. 118*, 5702−5707.
16. Andersen, J. F., Champagne, D. E., Weichsel, A., Ribeiro, J. M. C., Balfour, C. A., Dress, V., and Montfort, W. R. (1997) *Biochemistry 36*, 4423−4428.
17. Kaneko, Y., Yuda, M., Iio, T., Murase, T., and Chinzei, Y. (1999) *Biochim. Biophys. Acta 1431*, 492−499.

18. Weichsel, A., Andersen, J. F., Roberts, S. A., and Montfort, W. R. (2000) *Nat. Struct. Biol. 7*, 551−554.
19. Lakowicz, J. R., and Weber, G. (1973) *Biochemistry 12*, 4171−4179.
20. Johnson, K. A. (1992) in *The Enzymes, 3rd Ed.: Mechanisms of Catalysis* (Sigman, D. S., Ed.), Academic Press, New York.
21. Olson, J. S. (1981) *Methods Enzymol. 76*, 631−651.
22. Langsetmo, K., Fuchs, J. A., Woodward, C., and Sharp, K. A. (1991) *Biochemistry 30*, 7609−7614.
23. Bisig, D. A., DiIorio, E. E., Diederichs, K., Winterhalter, K. H., and Piontek, K. (1995) *J. Biol. Chem. 270*, 20754−20762.
24. Sharma, V. S., and Magde, D. (1999) *Methods 19*, 494−505.
25. Romberg, R. W., and Kassner, R. J. (1979) *Biochemistry 18*, 5387−92.
26. Andersen, J. F., and Montfort, W. R. (2000) *J. Biol. Chem.* (in press).
27. Springer, B. A., Sligar, S. G., Olson, J. S., and Phillips, G. N. (1994) *Chem. Rev. 94*, 699−714.
28. Mansy, S. S., Olson, J. S., Gonzalez, G., and Gilles-Gonzalez, M. A. (1998) *Biochemistry 37*, 12452−7.
29. Carver, T. E., Rohlfs, R. J., Olson, J. S., Gibson, Q. H., Blackmore, R. S., Springer, B. A., and Sligar, S. G. (1990) *J. Biol. Chem. 265*, 20007−20020.
30. Shaw, A. W., and Vosper, A. J. (1976) *J. Chem. Soc., Faraday Trans.*, 1239−1244.
31. Kerwin, J. F., Jr., Lancaster, J. R., Jr., and Feldman, P. L. (1995) *J. Med. Chem. 38*, 4343−62.
32. Rohlfs, R. J., Mathews, A. J., Carver, T. E., Olson, J. S., Springer, B. A., Egeberg, K. D., and Sligar, S. G. (1990) *J. Biol. Chem. 265*, 3168−3176.
33. Gibson, Q. H., Regan, R., Elber, R., Olson, J. S., and Carver, T. E. (1992) *J. Biol. Chem. 267*, 22022−22034.
34. Kholodenko, Y., Gooding, E. A., Dou, Y., Ikeda-Saito, M., and Hochstrasser, R. M. (1999) *Biochemistry 38*, 5918−5924.
35. Gibson, Q. H., Olson, J. S., McKinnie, R. E., and Rohlfs, R. J. (1986) *J. Biol. Chem. 261*, 10228−10239.
36. Carver, T. E., Olson, J. S., Smerdon, S. J., Krzywda, S., Wilkinson, A. J., Gibson, Q. H., Blackmore, R. S., Ropp, J. D., and Sligar, S. G. (1991) *Biochemistry 30*, 4697−4705.
37. Gong, W., Hao, B., Mansy, S. S., Gonzalez, G., Gilles-Gonzalez, M. A., and Chan, M. K. (1998) *Proc. Natl. Acad. Sci. U.S.A. 95*, 15177−15182.
38. Paesen, G. C., Adams, P. L., Harlos, K., Nuttall, P. A., and Stuart, D. I. (1999) *Mol. Cell 3*, 661−71.
39. Champagne, D. E., Nussenzvieg, R. H., and Ribeiro, J. M. C. (1995) *J. Biol. Chem. 270*, 8691−8695.

BI000766B